Experimental Studies of Dynamic Behavior of TiNi Alloy Thin Circular Plate subjected to Transversal Impact

Abstract

Here goes the abstract. For instance, one can write that this work The experimental research of thin circular plate of pseudo-elastic TiNi alloy under fixed supports and transversal impact loading was conducted through using the modified apparatus of Split Hopkinson Pressure Bar. The experiment results of pseudo-elastic TiNi alloy was compared with that of A3 steel. The nature of dynamic mechanical response of the structure in spatio-temporal scale, including the propagation of flexible wave in the plate, evolution of transformation zones and full-field out of plane displacement were derived. The results show that transformation zones and transformation hinge may generate near the center of the plate (about 5mm) because of two-dimensional diffusion effect of the circular plate under impact loading. The transformation hinge disappears after unloading; however, the A3 steel plate has residual deformation obviously. The impact response of TiNi alloy thin circular plate is dominated by the thermo-elastic martensite phase transformation and inverse transformation, which differs from the conventional elastic-plastic transformation mechanism.

Cui Shitang [a]
Wang Bo [a]
Tang Zhiping [a]
Zhang Ke [a,*]

[a] CAS Key Lab for Mechanical Behavior and Design of Materials, University of Science and Technology of China, Hefei 230026, Anhui, P.R. China

[*] Corresponding author email: zhangke@ustc.edu.cn

1 INTRODUCTION

Phase transformation can greatly affect the mechanical response of materials and structures, since the transformed material becomes a new material indeed. This is a common concern in material science, solid mechanics and industry nowadays. Shape memory alloy (SMA), is a new smart material with unique pseudo-elastic (PE) and shape memory effect (SME). The TiNi alloy in PE state can absorb tremendous energy with the phase transformation hysteresis without residual deformation when the load removed. It has manifested potential advantage in the anti-earthquake pro-

tection and impact absorption for engineering structures and been applied to the impact-resistant composite material field. Paine and Rogers (1994) discover that despite merely 2.8% of SMA fiber in the total volume, it can vastly enhance the impact- resistant and energy absorbing property for composite material beams. The research of Birman (1996) et al indicates that the deflection of carbon/epoxy laminates containing SMA fiber can reduce by about 1/3 under the low speed impact. Scholars such as Mi-Sun Rim (2011) also draw the similar experiment conclusions.

In recent years, many scholars have researched the dynamic mechanical behaviors of material with phase transformation. The work regarding the impact structural response with phase transformation has rarely been reported so far. Guo et al (2005) conducted Taylor impact experiment on TiNi alloy rod with phase transformation. Lagodas (2003) and Dai et al (2004) also researched the propagation of phase transition wave and phase boundaries propagating along SMA rods. Li Dan (2007, 2012) conducted systematic experiment and numerical simulation research on the mechanical behavior of TiNi alloy cylinder shell under the axial impact. Tang et al (2008, 2012) conducted a study on the dynamic response of TiNi alloy beam in PE state with a rectangle cross-section under transversal impact experimentally. They found the strain concentration caused by the thermo-elastic martensitic phase transition on the fixed end and defined it as "Phase Transformation Hinge (TH)". The TH can disappear due to reverse phase transition and a PE beam has no residual deformation after the unloading process, which differs from the conventional "Plastic hinge (PH)". However, this previous work was preliminary and needed further study. In this paper, thin circular plates of TiNi alloy, as a typical 2D structure, are selected for the transversal impact experiments. For comparison steel plates of the same size are also studied. The purpose of the present study is to explore the wave response and dynamic structural response of TiNi alloy plates subject to transversal impact at various time stages and to compare with elastic-plastic of the same geometry.

2   TRANSVERSAL IMPACT EXPERIMENTS FOR TINI PLATES

2.1 Specimens' Size and Experimental Methods

Experiments were conducted on the modified $\Phi37mm$ Split Hopkinson Pressure Bar(SHPB) as displayed in Fig. 1. The TiNi alloy plate sample in PE state is $220 \times 220 \times 2mm^3$ in size and 12 M10 pre-stressed bolts are fixed between two steel plates 10mm in thickness, which are fixed on the track. A round hole of $\Phi180mm$ lies at the center of the plate as the actual experiment size of the plate sample. The momentum of the bullet from a gun has been transferred to the impact projectile via the input bar. For simplicity, the impact projectile will be called projectile below. Two sizes of projectiles are used. The head of the both types are semi-sphere to ensure the point contact in the collision. The first type is 10mm in diameter, 100mm in length, and 117 g in mass. The second one is 14mm in diameter, 200mm in length, and 237 g in mass. Both types are made of 45# steel and the surface rigidity is enhanced through heat treatment. The high-speed camera CCD1 (Phantom v7.1) was used to record the process of bullet collision at the frequency of 10000 fps to observe the interaction between bullets and plate and to obtain various projectiles speeds over the time.

The distribution of deflection for the whole plate was measured by shadow moiré method. The grid was placed 10mm before the pate and the pulse xenon bulb was used to be light source. The dumb white paint was coated on the surface of the sample in order to increase the contrast of the

moiré image. The high speed camera CCD2 (Phantom V12.1) was used to record the change of moiré at the frequency of 50000fps. After the plate deformation, the formula for calculation the Nth stripe (D. Kokidko, 1997) is

$$w_N = \frac{NL}{(D/P) - N} \tag{1}$$

N is the fringe number, P=0.02mm is the grating pitch (distance between the centers of two adjacent lines), D is the distance between light source and the camera, L is the distance between grid and light source, as shown in Fig 1.
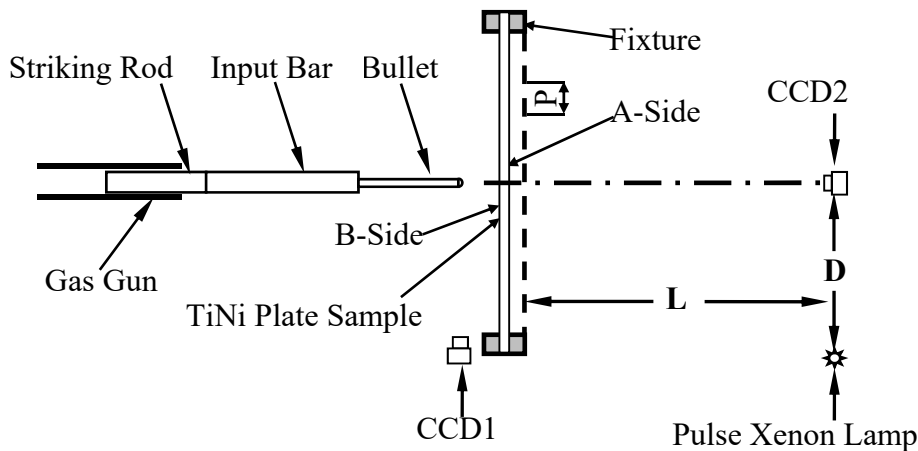
Figure 1: Set up for TiNi alloy plate transverse impact experiment.

The local dynamic correspondence of the sample is measured by the strain gauges and strain measurement system consists of the strain gauge, dynamic strain gauge and digital oscilloscope. The strain gauges on the plate were the plastic strain gauges model BX120-1AA made by Huangyan Strain Gauge Company, which can measure large strain up to 10% and the sensor size is 1 mm x 1 mm. Altogether 11 strain gauges are attached to the plate as displayed in Fig. 2. The code A on the gauge stands for the free end of the sample, B stands for loading end. The first number stands for the location of the gauge with "1, 2, 3, 4" respectively 5mm, 30mm, 55mm and 85mm to the center of the plate. For the second number, "1" and "2" stand for the radial and circumferential directions respectively with the gauge A_0 attached to the center of the plate. In addition to A_0, the gauge should be symmetrically attached to the two sides of the plate, i.e. A and B, to observe the symmetrical property of the strain signals on the two sides of the plate. The strain signals were input into the ultra dynamic strain amplifier (Model WA-02), and recorded by three digital oscilloscopes, in which two oscilloscopes (Model TDS3034B) and the other oscilloscope (Model TDS654C) and 5points/μs are used to record the strain wave profiles during the impact. When the bullet moves to 5mm from the plate, TTL loop is used to trigger the pulse xenon bulb, causing powerful pulse when discharging. The three oscilloscopes were all used the pulse xenon charging as the signal for trigger, so as to make a uniform timeline for the strain waves.

(a) Strain gauges at A side   (b) Strain gauges at B side
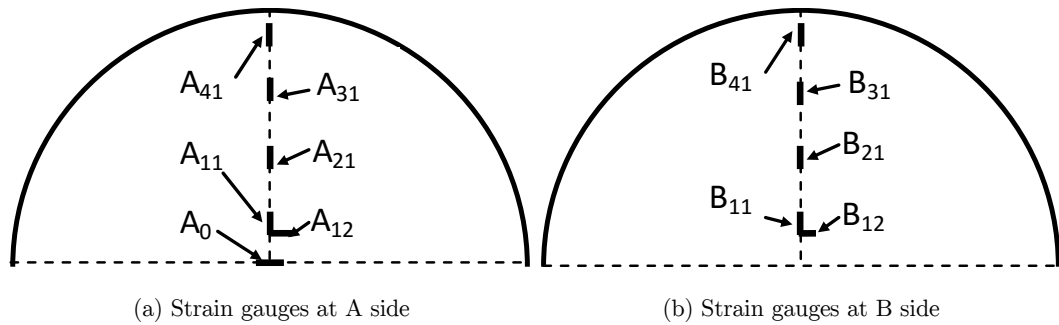
Figure 2: TiNi plate and sketch of strains gauges' location.

2.2 The Material Properties of TiNi Alloy Plate

The TiNi alloy plate was bought from Beijing Jiyi Science Commercial Co, Ltd. The composition of the TiNi alloy used in the experiments was Ti-50.9at%Ni, and its density was 6450 kg/m^3. The material is in the state of austenite in the room temperature. Under the one-dimension stress condition at the room temperature, the stress-strain curve obtained through MTS has obvious hysteretic and small residual deformation when unloaded as shown in Fig. 3. In accordance with this figure, the material mechanical parameters of TiNi alloy are that: the elastic modulus of the austenite phase is 62 Gpa, the initial martensite phase transition stress and strain (at point A) are σ_{im}=460Mpa and ε_{im}=0.75%, the finish martensitic phase transition stress and strain (at point B) σ_{fm}=545Mpa and ε_{fm}=4.75%, the initial stress and strain for reverse transition (point D) are σ_{ir}=230Mpa and ε_{ir}=3.82%, the finish stress and strain for reverse transition (point E) are σ_{fr}=160Mpa and ε_{fr}=0.25%, respectively. Phase transition strain i.e. the width of the plateau is 4.0%.
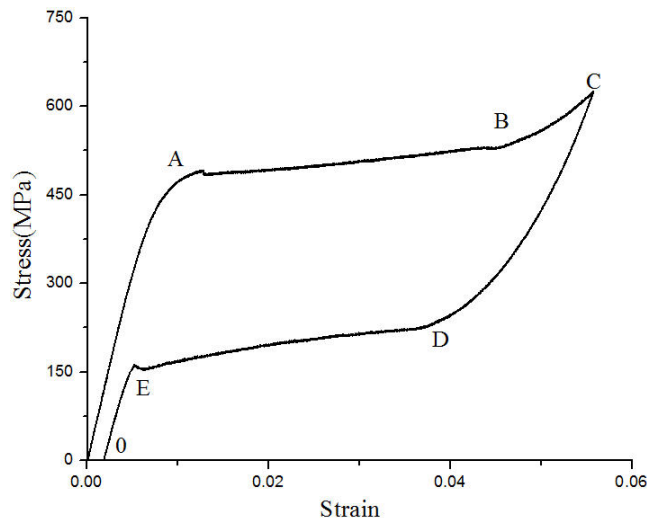
Figure 3: Quasi-static stress-strain curve of TiNi alloy of PE state at room temperature.

3 EXPERIMENT RESULTS OF TINI ALLOY PLATE SUBJECTED TO TRANSVERSAL IMPACT

3.1 Experimental Summary

The transversal impact experiment on TiNi alloy plate in PE state under fixed supported were conducted 9 times, the first bullet was used for seven and the second one used for the other two. The codes and the results of the experiments are shown in Table 1. For convenience, two impact experiments were conducted on A3 steel plate under the same conditions. TiNi alloy plate show no remaining deformation at the end of the experiment, but A3 steel plate show apparent deformation. The remaining deflection at the center of plate in experiment 8 and 11 are 0.49mm and 0.47mm respectively.

Exp No	Specimens	Bullet No	V_0(m/s)	V_1(m/s)	Def(mm)	ε_{max} (%)	η(%)
1	TiNi-1	1	8.16	6.39	2.90	0.74	38.67
2	TiNi-2	1	9.30	7.62	3.10	0.93	32.86
3	TiNi-3	1	7.80	6.04	2.60	0.70	40.04
4	TiNi-4	1	9.63	7.72	3.40	1.01	35.73
5	TiNi-1	1	9.80	8.05	3.42	1.21	32.02
6	TiNi-2	1	9.88	8.01	--	1.10	34.27
7	TiNi-3	1	8.82	7.12	2.94	0.85	34.83
8	Fe-1	1	8.64	5.45	2.53	--	57.24
9	TiNi-4	2	4.74	3.56	3.01	2.27	43.59
10	TiNi-1	2	5.33	4.23	4.56	2.80	37.02
11	Fe-2	2	4.74	2.70	2.53	--	67.55

Note: (1) "-"means data not measured. (2) The same specimen number means the specimen was used again. (3) V_0 denotes the projectile velocity. (4) V_1 denotes the residual projectile speed.

Table 1: Summary of dynamic experiments performed on TiNi and steel plates.

Experiment 9 is typical, in which the bullet impacts on TiNi alloy plate at the speed of 4.74m/s, so CCD1 image will be examined in this case. Fig 4 reflects some details of the interaction between the bullet and the plate through the interpretation of CCD1 image to determine how the speed and movement of the bullet vary with time. After the impact of the plate (a point), the bullet will be resisted by the plate and decrease in speed. The kinetic energy at the center of the plate will spread radially on the plate, and then the bullet pushes the plate to move forward. At about 0.7ms (b point), the bullet flies almost at the even speed, indicating short disengagement between the bullet and the plate. In the movement of the plate, more kinetic energy is converted to deformation energy (elastic deformation or phase change) and the speed at the plate center decreases. At 0.80ms (c point), the bullet impacts on the plate again and the bullet moves with the plate. At 1.24ms (d point), the plate reaches the max deflection, i.e. 3.10mm, and then the plate begins to rebound and the bullet begins to reverse as pushed by the plate. At 1.60ms (e point), there is a short disengagement between them for about 0.20ms. At 1.80ms (f point), the plate catches the bullet and another collision happens, until 2.20ms (g point) when the bullet flies at even speed and disengages with plate completely, and then the collision is over. At this time, the plate begins the free vibration.
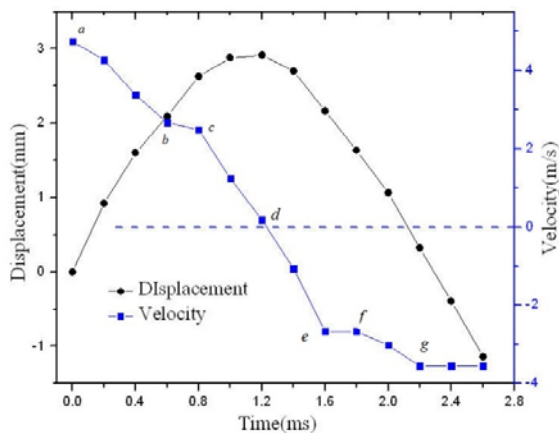
Figure 4: Velocity and displacement curves of bullet.

3.2 The Distribution of Deflection of the Plate During the Process of Impact

Fig 5 is part of moiré image of typical experiment 9 taken by CCD2. The distribution of full-field deflection and evolution at different times during the impact process obtained based on the moiré image through formula (1).

| (1) 0.26ms | (2)0.30ms | (3)0.40ms | (4)0.50ms |

| (5)0.60ms | (6)0.70ms | (7)0.80ms | (8)0.86ms |

| (9)0.90ms | (10)1.00ms | (11)1.10ms | (12)1.20ms |

(13)1.24ms   (14)1.30ms   (15)1.34ms   (16)1.40ms

(17)1.50ms   (18)1.60ms   (19)1.70ms   (20)1.80ms

(21)1.90ms   (22)2.0ms   (23)2.1ms
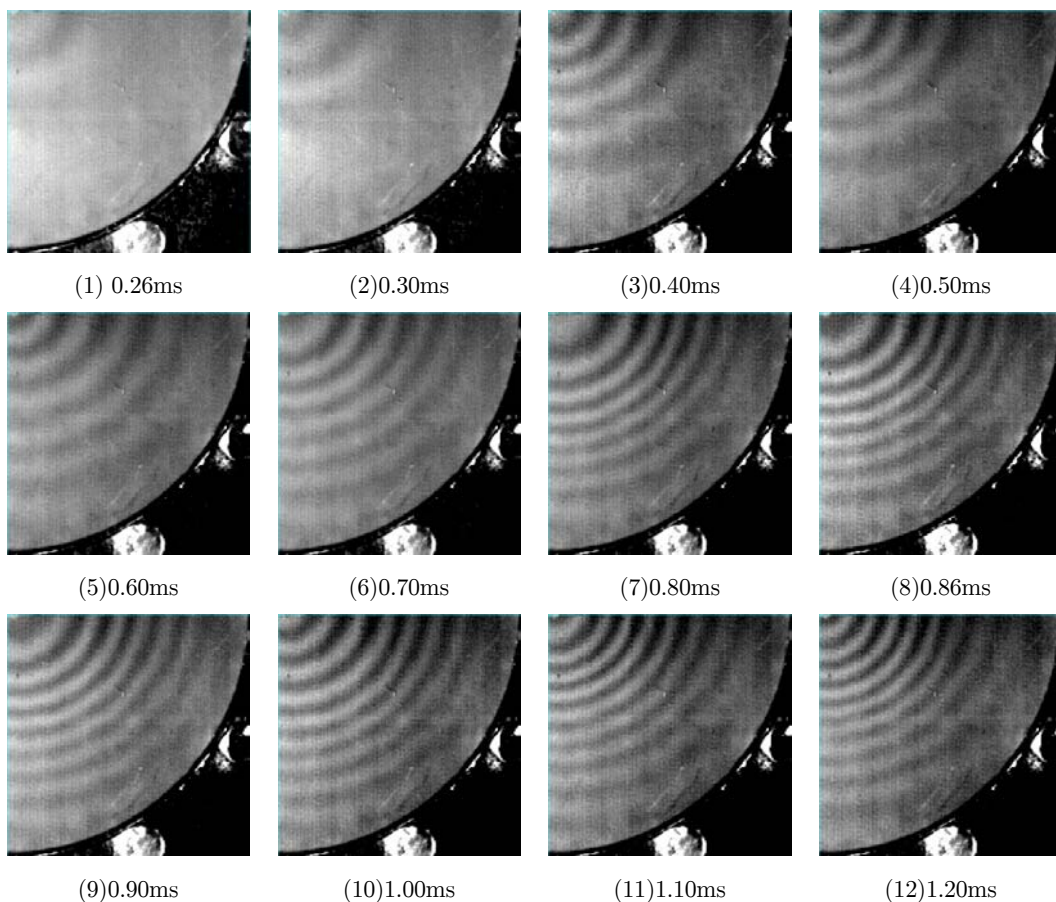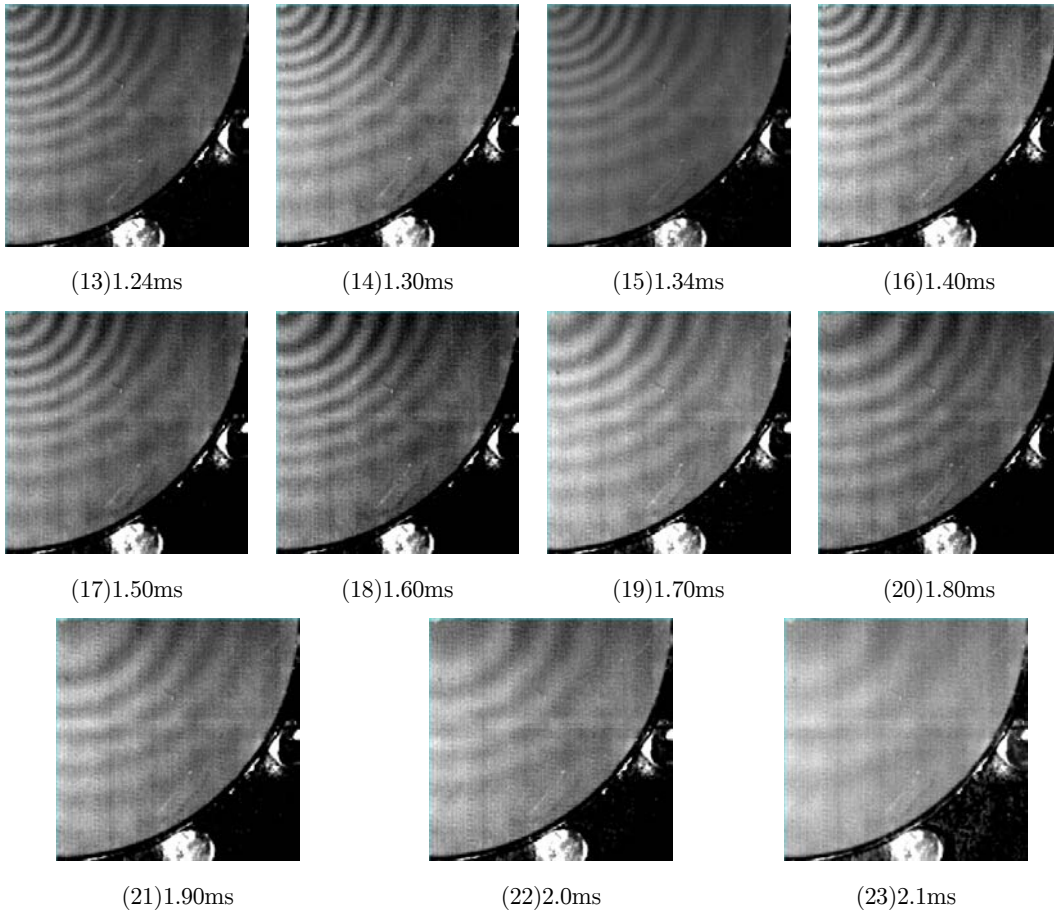
Figure 5: High speed photograph of transient deformation of using shadow moiré.

(a)   (b)

(c)
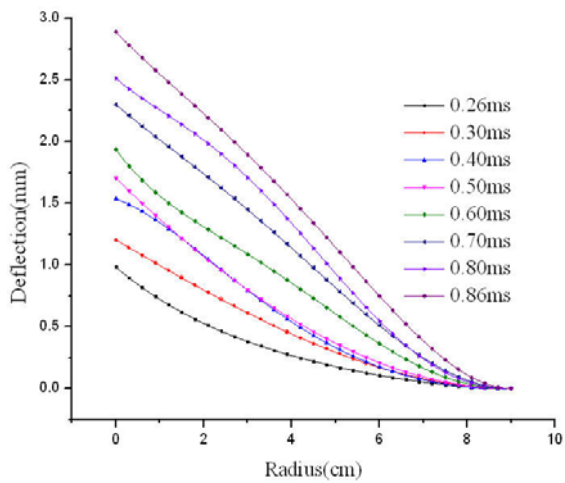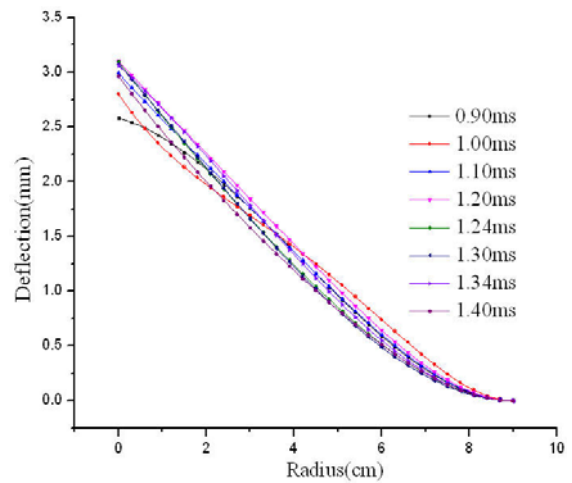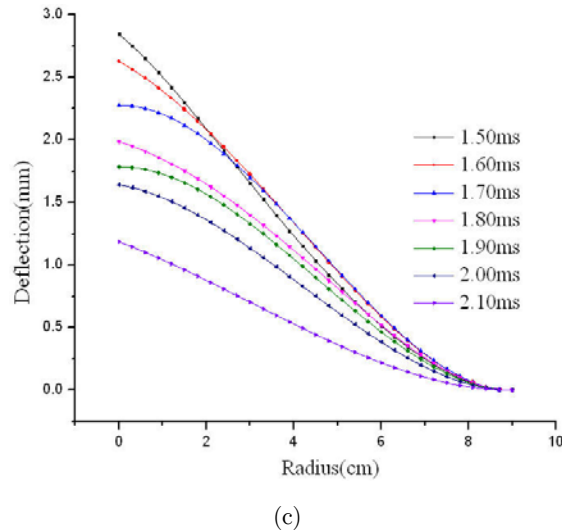
Figure 6: Displacements obtained from shadow moiré method.

3.3 Stress Waves Propagation in Plates

After the bullet collides with the plate at a constant speed, the flexible wave and a shear wave propagation into the plate and make it move and deform. It meanwhile propagates a compression wave to the bullet and decreases its speed. Since the shear wave amplitude is relatively small, the deformation of the plate is mainly caused by flexible wave (Jones, N. , 2010). The interaction between the bullet and the plate and the contact state of the collision point are determined by the propagation and interaction of the wave in the bullet and the plate. The local dynamic response of the plate and the wave propagation are reflected from the 11 strain gauge signals at different positions and locations on both sides of the sample.

Firstly, the response to the load segments is analyzed. Select A_0 on A side (free side) and "1" radial strain and it can be seen that A_0 reaches a maximum of 2.27% at about 1.24ms, while the maximum of "1" is only 0.66% in radial strain with a slight delay. It can be seen that the amplitude declines rapidly along its radial direction due to the two-dimensional effect of the plate when the flexible wave propagate outward from the center. Since waves are complex and interacting with each other in the process of the impact, it is difficult to prevent the propagate of the flexible wave from interruption. The strain signal "2", "3" and "4" are the combined effect of the waves.

Careful observation of the recorded waves reveals the following characteristics: (1) The strain waves at "1", "2", "3", "4" on both sides of A and B are symmetrical, only with a slight difference on the strain amplitude, indicating that the dynamic bending response is mainly shown. (2) All waves are superimposed high-frequency oscillation about 77μs in period, and the period and wave have the same time span back and forth in the bullet, indicating that the high frequency oscillation is caused by the propagation in the bullet. (3) In terms of the spatial distribution, the strain signals "2", "3" and "4" are relatively small (<0.2%), far below the phase transition critical strain 0.75%. It can be speculated that the region 30mm outside the plate center is elastic without phase transition in the entire process of impact. The maximum strain signal at A_0 is far more than the phase transition

critical strain, whereas the signal at A_{12} is a little above it, indicating that the phase transition zone may be distributed slightly larger than 5mm. (4) In terms of the time domain process, despite the complex waves in the plate, we can, in accordance with the strain transmission signal at A_0, divide the dynamic structural response in the impact process into three phases as shown in Fig 7a. (0-1.24ms) stands for load segment; A_0 strain signal shows the overall increasing trend. (1.24ms-2.36ms) stands for unloading segment; A_0 strain signal shows the overall decreasing trend, in which the amplitude increase of strain signal after 1.80ms is generated by the collision between the plate and the bullet again, (after 2.36ms) stands for free vibration segment, and the strain signal shows cyclical changes.
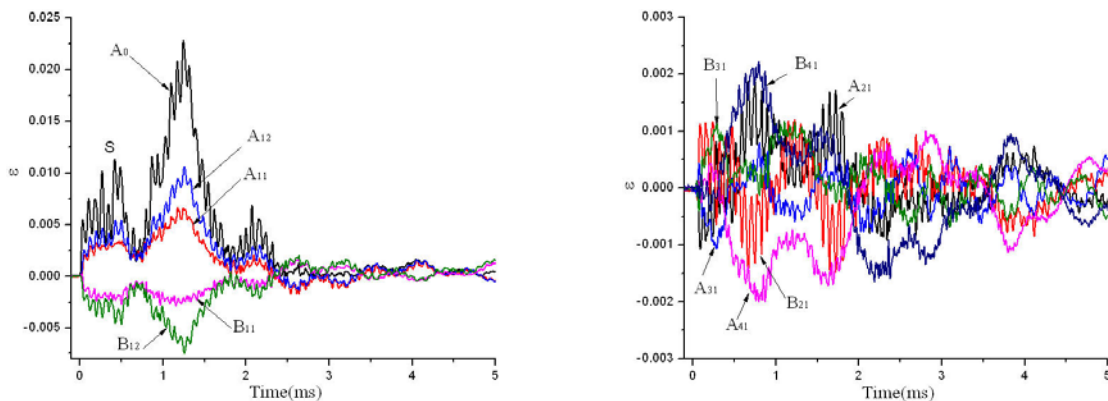
a) Strain wave profiles of A0、A11、A12、B11 and B12   b) Strain wave profiles of A31、B31、A41 and B41

Figure 7: Strain wave profiles of experiment 9.

Figure 8 shows the strain waves of A_0, A_{21}, A_{31} and A_{41} within 0.2ms. Except A_0, in the head of each strain signals the positive and negative alternate with amplitude and cycle increasing gradually, reflecting the character of dispersion of bending waves. The experimentally measured material parameters can be used to calculate the velocity of TiNi alloy elastic bending wave head as 1,783m/s (R. D. Mindlin 1951). According to Figure 8, the jumping time t_0, t_1, t_2, t_3, t_4 can be obtained for A_0 and A_{21}, A_{21} and A_{31}, A_{31} and A_{41} to calculate the wave velocity of C_{02}, C_{23} and C_{34} for the three segments are respectively 1739m/s, 1732m/s and 1698m/s. The trend is decreasing and the average values are 1723m/s, basically consistent with the theoretical velocity (slightly smaller). The round trip between the impact center and the plate boundary consumes about 100μs. Generally, after 3-5 round trips (about 0.3-0.5ms, corresponding to S point in Figure 7a) can we regard that the sample transits from wave response to dynamic structural response. That is, point S divides the plate response into wave response and structural response. Fig. 4 is the curve of bullet movement and speed as recorded by high-speed CCDI. The bullet speed change is small in the response (0.5-0.8s), indicating the short disengagement too.
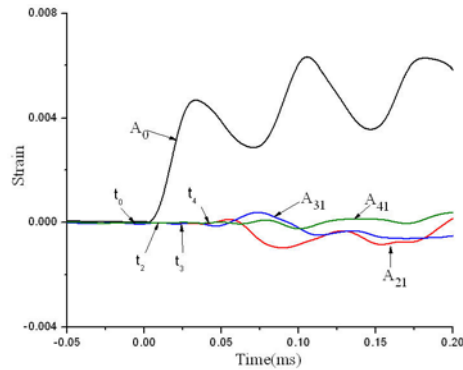
Figure 8: Strain wave profiles of A0、A21、A31 and A41 in 0.20ms.

Due to the consistently complex stress state inside the plate during the impact process, it is impossible to determine whether the material undergoes a phase change by using maximum stress or strain. Therefore, we use the equivalent strain to observe the phase change in the plate (Auricchio, 2001).

$$\varepsilon_{eq} = \frac{1}{\sqrt{2}(1+\mu)}\sqrt{\left(\varepsilon_r - \varepsilon_\theta\right)^2 + \left(\varepsilon_\theta - \varepsilon_z\right)^2 + \left(\varepsilon_z - \varepsilon_r\right)^2} \tag{2}$$

In which εx, εy, εz are main strain and μ is Poisson's ratio.

Under the simple stress condition experimentally determined by MTS axial tensile stress, the initial martensitic phase transition strain and the finish martensitic phase transition strain are respectively 0.75% and 4.75%, while the initial strain and the finish strain for reverse transition are respectively 3.82% and 0.25%. Under the complex stress state, the corresponding equivalent initial martensitic phase transition strain and the finished martensitic phase transition strain are the same with those in uniaxial tension, respectively.

Figure 9 is an equivalent strain diagram for A_0 and the two sides of A and B within 3ms. In this figure, the following points can be seen: (1), at 0.26ms (a point), the equivalent strain at A_0 firstly exceeds the phase transition critical strain, indicating that the central surface material of the A side undergoes a change from austenite to martensite with a large amplitude fluctuations. At 0.854ms (b point), equivalent strain at A_0 again exceeds 0.75%, indicating that the central material reenters the phase change state. The plate is then driven by the bullet; while the equivalent strains at A_0 and "1" on the A side is on the increase, indicating that the phase boundary spreads outward from the center. Phase transition at "1" on A side at the time of 1.256ms is 0.79% as maximum, exceeding the phase transition critical strain, indicating the A-side phase transition zone has spread to 5mm from the center, which can be used to approximately calculate the average velocity of about 12.4m/s under the impact in the phase change area (boundary). (2), at "1" on the B side, the maximum equivalent strain is only 0.50%, indicating that the phase transition has not occurred, while both sides of the phase transition zone are asymmetric and the stretching side is larger than the compression side, which is due to the tension compression asymmetry and the local membrane force. (3), the maximum equivalent strain at A_0 is 1.80% (d point), while is only 0.79%, at "1", showing that the radial flexible wave amplitude declines greatly due to the two-dimensional effect. (4), At 1.092ms (c point), the equivalent

strain reaches 1.50% at A_0, more than two times of the equivalent phase transition critical strain, indicating that the phase transformation hinge is formed at the center of A side and this area will undergo the main deformation and energy absorption effect.
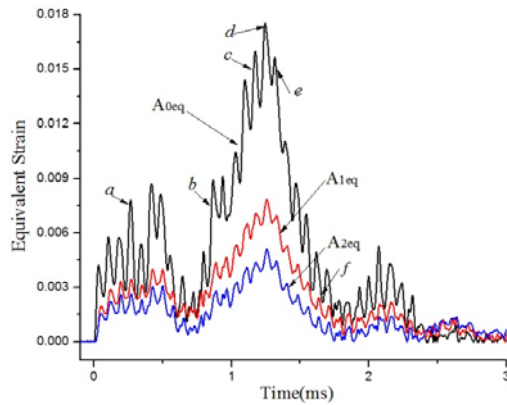
Figure 9: Equivalent Phase Change at A0, A1 and B1 within 3ms.

3.4 Transversal Impact Behavior of Steel Plate

Attach large plastic strain gauges on the steel plate and the strain gauge positions, naming rules and the measurement methods are the same with TiNi alloy plate. In experiment 11, bullet 2 is used to impact on the center of A3 steel plate with full clamped at the speed of 4.74m/s. Fig. 10 is the strain waveform recorded in experiment 11. The strain waves at the opposite positions on the sides of A and B are substantially symmetric; A -side amplitude is slightly large and both sides of the circumferential strain is significantly greater than the radial strain. Compared with the waveforms of TiNi plate wave in experiment 7, strain wave in experiment 11 is smooth. At "2" and "3" on both sides, the radial strain is relatively small ($< 0.2\%$) , so it can be speculated that "2" and "3" are still in elastic state. The dynamic response of steel bullet impact can also be shown in Figure 10(a) as divided into three stages, the loading segment (0-0.894ms), unloading segment (0.894ms-1.865ms) and free vibration segment (after 1.865ms).
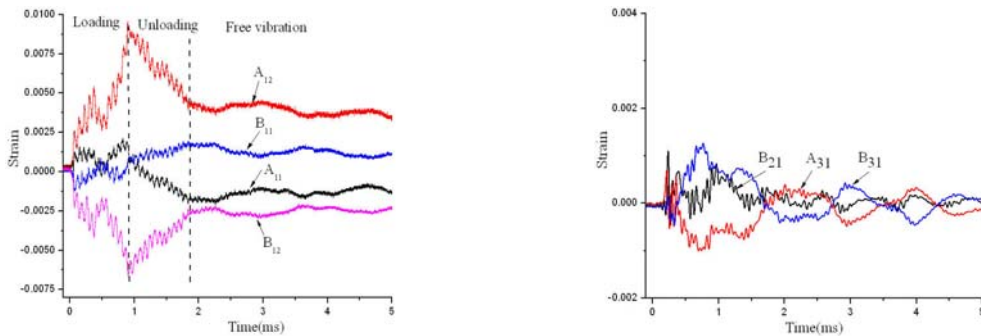
(a) Strain wave profiles of A11、A12、B11 and B12   (b) Strain wave profiles of A31、A41、B31 and B41

Figure 10: Strain wave profiles of EXP 11.

Figure 11 provides the curve of the equivalent strain varying with the time within 3ms at "1" on the sides of A and B. It can be seen that from about 0.5ms, the value of A is larger than that of B side mainly because of the large membrane force here. At 0.894ms, both sides reach the maximum equivalent strain, i.e. 0.57% and 0.46%, much larger than the critical equivalent plastic strain. It can be assumed that the radius of the plastic zone formed at the center of the plate in the process of loading exceeds 5mm. Once the plastic zone is formed, it will undergo the major deformation and absorb most of the energy in the plate.
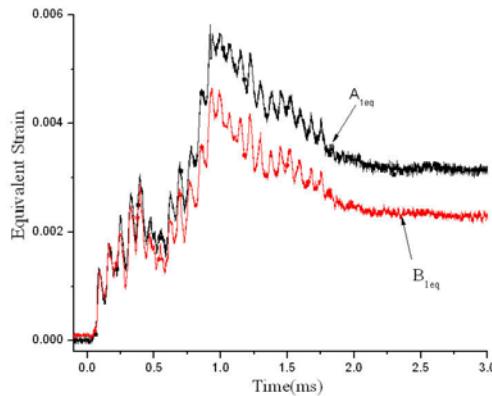
Figure 11: Equivalent strain of A1 and B1 in 3ms in EXP 11.

The unloading phase lasts for 0.971ms, slightly longer than the loading time. At 1.865ms, unloading process is completed, and then the residue equivalent strain on both sides (A and B) is 0.34% and 0.26%, thus forming a permanent plastic zone, and the plastic zone is presumably not less than 5mm in radius. After 1.865ms, it is shown in the high-speed CCD1 image that the bullet disengages from the board completely and the plate is in a free state of vibration. The sample recovered indicates the residual deflection at the plate center is 0.47mm.

4 CONCLUSIONS

By using a modified SHPB apparatus, the transversal impact experiments through the approach of shadow moiré and foil gauge on the dynamic mechanical behaviors of pseudo-elastic TiNi alloy thin circular plate under the conditions of fixed support have been conducted and analyzed, and compared with the A3 elastic-plastic steel plates. The experimental results show the following conclusions.

(1) Under shock loading conditions, the early response of TiNi alloy plate is mainly the wave response of the flexible wave propagation. After the propagation of the flexible wave for 3-5 round trips in the plate (about 0.5ms), it gradually transits to the dynamic structural response.

(2) During the impact process, a local phase transformation hinge area is formed at the center of the TiNi plate, in which the strain and energy absorption concentrate, and the rest part is released to some degree. After unloading, the phase transformation hinge area in TiNi alloy plate disappears, but that in the steel sample does not disappear. For PE plate under the present experimental condition, only a local TH is formed at the center of the plate when the plate suffers from an impact.

(3) After the impact experiment a PE TiNi alloy plate can recover to its original position without residual deformation, while a steel cantilever produces a permanent residual deformation which increases with the maximum deflection achieved during impact.

(4) The impact properties of TiNi alloy plates in pseudo-elastic state are governed by the thermo-elastic martenstic phase transition, their intrinsic features differ from the elastic－plastic behavior of steel specimens.

Acknowledgements

References

Auricchio, Sacco. (2001). Thermo-mechanical modeling of a super-elastic shape – memory wire under cyclic stretching-bending loadings. International Journal of Solids and Structures 38:6123-6145.

D. Kokidko, L. Gee, S. C. Chou et al. (1997). Method for measuring transient out-of –plane deformation during impact. International Journal of Impact Engineering 19(2):127-133.

Dai XY, Tang ZP, Xu SL, Guo YB, Wang WQ. (2004). Propagation of macroscopic phase boundaries under impact loading. International Journal of Impact Engineering 30: 385-401.

Dan Li, Zhiping Tang, Xinhua Zhang. (2007). Dynamic buckling of super-elastic SMA shells under axial impact-numerical simulation. Proceedings of the 7th International conference on shock and impact loads on structures 335-342.

Guo YB, Tang ZP, Zhang XH, Xue SL. (2005). Phase transition taylor test. Impact loading of lightweight structures. WIT Trans EngSci 49: 241-255.

HUANG-He, TANG Zhi-ping. (2012). Investigation on Structural Dynamic Response of a Tini End Clamped Beam under Transversal Impact. Journal of Experimental Mechanics 27(1):93-101. (in Chinese)

Jones Norman ,Alves Marcilio. (2010). Post-failure behaviour of impulsively loaded circular plates. International Journal of Mechanical Sciences 52: 706-715.

Lagoudas DC, Ravi-Chandar K, Sarh K et al.(2003). Dynamic loading or ploy crystalline shape memory alloy rods. Mechanics Mater 35: 689-716.

Min-Sun Rim, Eun-Ho Kim, In Lee et .al. (2011). Low velocity impact characteristics of composite plates with shape memory alloy wires. Journal of theoretical and applied mechanics 49(3): 841-857.

Paine J S N , Rogers C A. (1994). The response of SMA hybrid composite materials to low velocity impact. Journal of Intelligent Material Systems and Structures 5(4): 530-535.

R. D. Mindlin. (1951). Influence of Rotatory Inertia and Shear on Flexural Motions of Isotropic Elastic Pates. Journal of applied mechanics 18: 31-38.

Victor Birman, K. Chandrashekhara, Sukhendu Sain. (1996). An approach to optimization of shape memory alloy hybrid composite plates subjected to low velocity impact. Composites Part B : Engineering 27(5):439-446.

ZHANG Xing-hua, TANG Zhi-ping, LI Dan et al. (2008). Experimental study of the Dynamic Structural Response of Pseudo-Elastic TiNi alloy Rectangular Cantilever Beam upon a Transversal Impact. Journal of Experimental Mechanics 23(1):44-52.

Zhiping Tang, Dan Li. (2012). Experimental investigation of axial impact buckling response of pseudo-elastic NiTi cylindrical shells. International Journal of Impact Engineering 39:28-41.